A Nonlinear Frequency-Domain Model of Passive Intermodulation in Microstrip Lines Supporting 3-D Topology

Wenbo Wang[®], Wenchao Chen[®], Senior Member, IEEE, Yimin Wang[®], Huali Duan[®], Shuai S. A. Yuan[®], Graduate Student Member, IEEE, and Wei E. I. Sha[®], Senior Member, IEEE

Abstract—Traditional modeling of passive intermodulation (PIM) for microstrip transmission lines is limited by the form of nonlinear source, the topology of the microstrip transmission line, and the computational complexity of the model. In this work, we propose a nonlinear coupled-wave model based on typical PIM modeling frameworks, in which the distributed nonlinear sources are rigorously derived using nonlinear mixing theory and formulated in the frequency domain to facilitate structural extension. Moreover, a self-consistent solution to the nonlinear model is proposed to efficiently capture complex nonlinear mixing and interaction in the microstrip transmission lines. The validity of the developed model is confirmed by the near-field measurements of PIM distribution along the microstrip transmission line, and the reverse and forward PIMs are also measured on various samples to further validate the accuracy of the proposed model. Finally, the nonlinear coupled-wave model is extended to a more general form with the aid of full-wave simulation in multiphysics software COMSOL, and the consistency between the nonlinear coupled-wave model and the full-wave version demonstrates the feasibility of structural extension. The PIM distribution and variation at the different bending positions in bent microstrip transmission lines are also analyzed.

Index Terms—Distributed nonlinearity, microstrip transmission line (MTL), nonlinear model, passive intermodulation (PIM).

I. Introduction

THE interference caused by passive intermodulation (PIM) near the receiving frequency band has become more significant due to the increasing sensitivity requirements of advanced mobile communication systems [1]. PIM refers to spurious spectral components that arise from weak nonlinearities in passive devices such as ferrite isolators and circulators

Received 12 December 2024; revised 14 February 2025 and 27 March 2025; accepted 31 March 2025. Date of publication 23 April 2025; date of current version 16 September 2025. This work was supported in part by the National Natural Science Foundation of China under Grant 61975177, Grant U20A20164, and Grant 62122067; and in part by Zhejiang Provincial Natural Science Foundation under Grant LR21F010003. (Corresponding authors: Wei E. I. Sha; Wenchao Chen.)

Wenbo Wang, Wenchao Chen, Yimin Wang, and Huali Duan are with the College of Information Science and Electronic Engineering, Zhejiang University, Hangzhou 310058, China, and also with Zhejiang University-University of Illinois Urbana Champion Institute, International Campus, Zhejiang University, Haining 314400, China (e-mail: wenbow@zju.edu.cn; wenchaochen@zju.edu.cn; yimin.20@intl.zju.edu.cn; hualiduan@zju.edu.cn).

Shuai S. A. Yuan and Wei E. I. Sha are with the College of Information Science and Electronic Engineering, Zhejiang University, Hangzhou 310058, China (e-mail: shuaiyuan1997@zju.edu.cn; weisha@zju.edu.cn).

Digital Object Identifier 10.1109/TMTT.2025.3558262

[2], [3], [4], [5], coaxial connectors [6], [7], [8], [9], [10], duplexers [11], [12], [13], and antennas [14], [15], [16], [17]. PIM is caused not only by the nonlinearity of metal contacts and materials [18] but also by any nonlinearity on the path of multiple high-power signals. It is worth noting that PIM products may result from the combined action of multiple physical mechanisms.

Microstrip transmission lines are widely used in planar and radio frequency integrated circuits (RFICs) due to their cost-effectiveness, reliability, and ease of integration. In practical applications, microstrip transmission lines are inevitably accompanied by the generation of PIM interference. Due to the complex physical origin of nonlinearity, many behavioral models are often used to predict the distribution of PIM [19], [20], [21], [22]. The existing research on the effects of copper foil structure, surface roughness, and foil–dielectric interface in printed transmission lines has shown that the PIM sources are nonlocally distributed along the signal path [23], and some PIM models based on electrothermal coupling and nonlinear resistance have been proposed [24], [25], [26], [27], [28]. These studies have greatly promoted the research on PIM generation in the microstrip transmission lines.

However, there are still some issues that deserve to be addressed in the PIM models. First, the forms of distributed nonlinear sources are not rigorous enough, and the analytical models based on transmission line equations in the time domain exhibit high computational complexity. Second, most PIM models adopt uniform transmission line equations, limiting their applicability to microstrip structures with arbitrary topology. Therefore, it is highly valuable to develop PIM models capable of supporting structural extension with low computational complexity, which could facilitate the optimization of PIM levels in various configurations of microstrip transmission lines. To the authors' best knowledge, few studies have endeavored to develop such PIM models that meet these aforementioned requirements.

In this article, a more rigorous form of the nonlinear source is derived based on the theory of nonlinear mixing and wave propagation and is coupled with the frequency-domain equation of the uniform transmission line to accurately exhibit the generation of nonlinear signals. Furthermore, a self-consistent numerical method is proposed, which integrates the linear electromagnetic field solution into the nonlinear

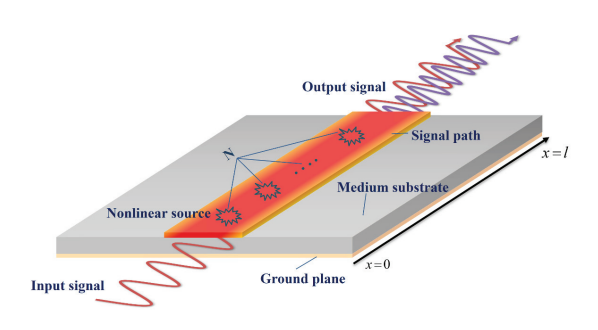


Fig. 1. Schematic of the nonlinear microstrip transmission line. The harmonic components arise due to N distributed nonlinear sources. The direction along the signal path is set as x-direction, and the length of the microstrip transmission line is l.

equation to solve for the PIM distribution. This approach not only reduces computational complexity but also facilitates the extension of PIM simulations to 3-D microstrip lines. Finally, the nonlinear coupled-wave model is implemented in the commercial software COMSOL to simulate PIM in 3-D microstrip lines with specific topological structures. This approach facilitates the investigation of low-PIM structure designs and the influence of multiphysics effects on PIM.

This article is organized as follows. The nonlinear coupled-wave model of microstrip transmission lines and the corresponding self-consistent solution are discussed in Section II. The practical validation of the proposed model is presented in Section III. The extension of the nonlinear coupled-wave model implemented by the COMSOL, and the PIM distribution and variation with different bending positions in bent microstrip transmission lines are explored in Section IV. The conclusion summarizes the main findings.

II. NONLINEAR COUPLED-WAVE MODEL AND SELF-CONSISTENT SOLUTION

This section presents the nonlinear coupled-wave model and the corresponding self-consistent numerical solution method. Initially, a more rigorous form of the distributed nonlinear sources is derived based on the theory of nonlinear mixing and interference. Building on this, the distributed nonlinear sources are incorporated into the uniform transmission line equations to capture the nonlinear PIM response in the frequency domain. Finally, a novel self-consistent numerical method is introduced to couple the linear solution with the nonlinear equations, iteratively refining the solution for the nonlinear components.

A. Modeling of Nonlinearity in Microstrip Transmission Lines

Considering a nonlinear microstrip transmission line excited by a two-tone signal, the harmonic components arise from the distributed nonlinear sources within the signal path, as shown in Fig. 1. Although the physical mechanisms underlying PIM generation in microstrip transmission lines may vary, the resulting PIM products stem from nonlinear motion or scattering of electrons within the signal path at the microscopic scale

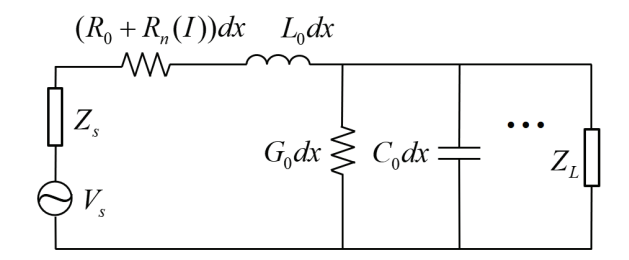


Fig. 2. Equivalent circuit model of the nonlinear microstrip transmission line. $R_n(I)$ is the nonlinear resistance, and dx is an infinitesimal element along the signal path of the microstrip transmission line.

and can be described macroscopically as the nonlinear conductivity of the microstrip transmission line [26], [29], [30]. Furthermore, PIM products in microstrip transmission lines originate from the nonlinear mixing and interaction between fundamental carrier components at each position according to the theory of parametric harmonic generation [31], highlighting the close relationship between the nonlinear sources and the fundamental carrier components.

Only one of the third order PIM products at $(2\omega_1 - \omega_2)$ is discussed in the following. Harmonic components of secondorder and higher generally have little effect on distortion at the frequencies of interest since they can be easily filtered out by filters. The analytical solutions for fundamental carrier currents $I(x, \omega_1)$ and $I(x, \omega_2)$ along the microstrip transmission line in the frequency domain take the form of $e^{\pm jk_1x}$ and $e^{\pm jk_2x}$, respectively, where k is the propagation constant. Therefore, the distributed nonlinear current sources generated by the nonlinear mixing should be written as C_n $I(x, \omega_1)$ $I(x, \omega_1)$ $I^*(x, \omega_2)$, where C_n is the nonlinear coefficient, so that the nonlinear current wave $I(x, 2\omega_1 - \omega_2)$ can rigorously satisfy the form of $e^{\pm j(2k_1-k_2)x}$ in terms of amplitude and phase. PIM signals depend on the type of source, which can be of voltage, current, or power type, and the voltage source is used in the following calculation. Therefore, the distributed nonlinear voltage source can be calculated as

$$U_{ns} = R_n I(x, \omega_1) I(x, \omega_1) I^*(x, \omega_2)$$
(1)

where R_n represents the nonlinear resistance of the microstrip transmission line, which is influenced by the nonlinear scattering effect from a microscopic perspective and can be affected by temperature, parameters of the manufacturing process, and fabrication tolerances [30], [32]. The nonlinear resistance R_n is simplified to a statistical parameter during calculation.

The equivalent circuit model of a uniform microstrip transmission line with distributed nonlinear voltage sources is shown in Fig. 2. The parameters R_0 , L_0 , G_0 , and C_0 are per-unit-length component parameters of the microstrip transmission line and can be extracted from S-parameters. Moreover, these component parameters are dispersive, so the corresponding component values should be applied at different frequencies.

To realize lower computational complexity compared to most existing analytical models built in the time domain, the nonlinear coupled-wave model for microstrip transmission lines is formulated in the frequency domain. Since the propagation of the nonlinear signal still satisfies the telegrapher's equations at the intermodulated frequency, the equations of the nonlinear microstrip transmission line are given as follows:

$$\frac{\partial U(x,\omega)}{\partial x}\bigg|_{\omega=2\omega_1-\omega_2} = -(R_0 + j\omega L_0)I(x,\omega) - U_{ns}$$
 (2)

$$\frac{\partial U(x,\omega)}{\partial x}\bigg|_{\omega=2\omega_1-\omega_2} = -(R_0 + j\omega L_0)I(x,\omega) - U_{ns} \qquad (2)$$

$$\frac{\partial I(x,\omega)}{\partial x}\bigg|_{\omega=2\omega_1-\omega_2} = -(G_0 + j\omega C_0)U(x,\omega) \qquad (3)$$

where the distributed nonlinear voltage source U_{ns} has been given by (1). By further differentiating all the terms in (3) with respect to x, and combining the result with (2), the resulting second-order differential equation for $I(x, 2\omega_1 - \omega_2)$ is given as follows:

$$\left. \frac{\partial^2 I(x,\omega)}{\partial x^2} \right|_{\omega = 2\omega_1 - \omega_2} = \gamma^2 I(x,\omega) + (G_0 + j\omega C_0) U_{ns} \quad (4)$$

where γ is the propagation constant and can be obtained as

$$\gamma = \sqrt{(R_0 + j\omega L_0)(G_0 + j\omega C_0)}|_{\omega = 2\omega_1 - \omega_2}.$$
(5)

It should be noted that (4) is an approximation because the PIM signals and carriers are not orthogonal in the power metric. Unlike fundamental carrier signals, the nonlinear harmonic signals in microstrip transmission lines are solely generated by distributed nonlinear sources without external excitation. Therefore, the boundary conditions for the nonlinear equations are given as follows:

$$Z_S(\omega)I(x,\omega) = \left(\frac{1}{j\omega C_0 + G_0}\right) \frac{\partial I(x,\omega)}{\partial x}\bigg|_{x=0}$$
 (6)

$$-Z_L(\omega)I(x,\omega) = \left(\frac{1}{j\omega C_0 + G_0}\right) \frac{\partial I(x,\omega)}{\partial x}\bigg|_{x=l}$$
(7)

where $Z_S(\omega)$ is the source impedance and $Z_L(\omega)$ is the load impedance at $\omega = 2\omega_1 - \omega_2$. If the nonlinear effect at the boundary is significant, the nonlinear current can be derived based on the specific nonlinear effects, and the strong nonlinear voltage source is then added at the boundary for calculation. Finally, the nonlinear harmonic voltage $U(x, 2\omega_1 - \omega_2)$ can be determined by (2) with the calculated $I(x, 2\omega_1 - \omega_2)$. The reverse PIM and the forward PIM are referred to as the PIM at circuit input and output ports, which can be determined as follows:

$$P_{\text{rev}} = \frac{1}{2} \text{Re} \{ I(0, 2\omega_1 - \omega_2) U^*(0, 2\omega_1 - \omega_2) \}$$
 (8)

$$P_{\text{forw}} = \frac{1}{2} \text{Re} \{ I(1, 2\omega_1 - \omega_2) U^*(1, 2\omega_1 - \omega_2) \}.$$
 (9)

B. Solution to the Nonlinear Coupled-Wave Model

Since the distributed nonlinear sources are coupled with the fundamental carrier components, the analytical solution of the nonlinear coupled-wave model is complicated. Therefore, a new self-consistent solution is proposed, and the solution process is given as follows. First, the finite-difference method (FDM) [33] is utilized to solve the numerical solution to fundamental carrier currents $I(x, \omega_1)$ and $I(x, \omega_2)$, so the distribution of nonlinear sources can be obtained by (1). Second, (4) is discretized into differential form so that the numerical solution to distributed nonlinear sources can be incorporated into it,

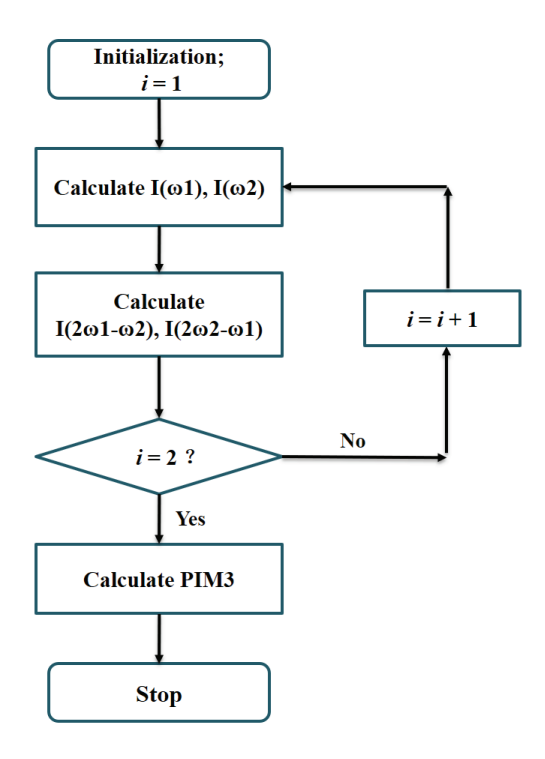


Fig. 3. Solution process of the nonlinear coupled-wave model for PIM generation in the microstrip transmission lines. The contribution of harmonic components to the fundamental carrier components is considered.

and then, the FDM is employed again to solve the nonlinear harmonic current $I(x, 2\omega_1 - \omega_2)$ and voltage $U(x, 2\omega_1 - \omega_2)$; the PIM products can be further calculated using (8) and (9). Finally, the linear component is corrected, and the nonlinear component is iteratively updated to ensure the self-consistency of the model. The flowchart illustrating the solution process of the nonlinear coupled-wave model is shown in Fig. 3.

More attention needs to be paid to calculating the fundamental carrier currents. In fact, the solution of the fundamental carrier currents $I(x, \omega_1)$ and $I(x, \omega_2)$ require iterative calculations because one fundamental carrier component can be regenerated by the mixing of nonlinear components with another fundamental carrier component in a nonlinear microstrip transmission line. Since the PIM product on the microstrip transmission line is typically more than 100 dB lower than the carrier power, it can be initially assumed that the nonlinearity makes little contribution to the generation of fundamental carrier components, and the self-consistent solution to the model will be performed later. Therefore, the nonlinear source is temporarily neglected when solving the fundamental carrier current distribution, thereby simplifying the equivalent circuit model of the microstrip transmission

The fundamental carrier voltages and currents along the microstrip transmission line in the frequency domain are determined by the following formulas:

$$\left. \frac{\partial U(x,\omega)}{\partial x} \right|_{\omega_1,\omega_2} = -(R_0 + j\omega L_0) I(x,\omega) \tag{10}$$

$$\frac{\partial U(x,\omega)}{\partial x}\bigg|_{\omega_1,\omega_2} = -(R_0 + j\omega L_0) I(x,\omega) \tag{10}$$

$$\frac{\partial I(x,\omega)}{\partial x}\bigg|_{\omega_1,\omega_2} = -(G_0 + j\omega C_0) U(x,\omega). \tag{11}$$

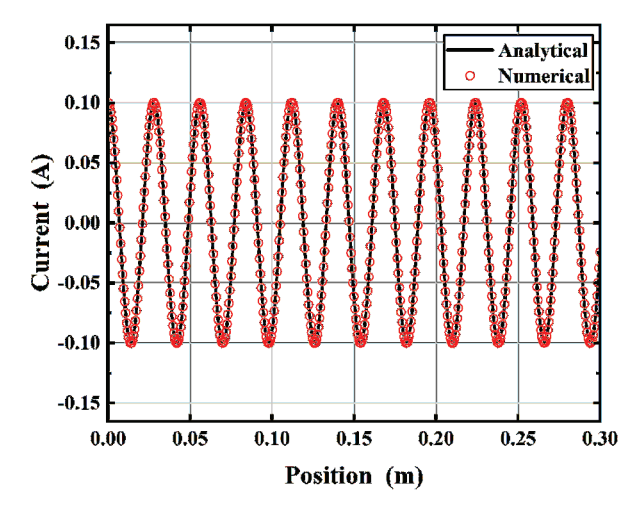


Fig. 4. Numerical and analytical solutions of fundamental carrier current along the microstrip transmission line. The analytical solution of the fundamental carrier current is consistent with that of the numerical solution.

Since the fundamental carrier components have the excitation of a two-tone signal at the ports, the boundary conditions at x = 0 and x = l are given as follows:

$$Z_{S}(\omega)I(x,\omega) - V_{s}\delta_{\omega} = \left(\frac{1}{j\omega C_{0} + G_{0}}\right) \frac{\partial I(x,\omega)}{\partial x}\bigg|_{x=0}$$
(12)
$$-Z_{L}(\omega)I(x,\omega) = \left(\frac{1}{j\omega C_{0} + G_{0}}\right) \frac{\partial I(x,\omega)}{\partial x}\bigg|_{x=l}$$
(13)

$$-Z_L(\omega)I(x,\omega) = \left(\frac{1}{j\omega C_0 + G_0}\right) \frac{\partial I(x,\omega)}{\partial x}\bigg|_{x=l}$$
(13)

where V_S is the source voltage and δ_{ω} is the impulse function at fundamental carrier frequencies ω_1 or ω_2 .

The microstrip transmission line is discretized into N sections for numerical calculation, and the spatial derivative of the current is replaced by the finite-difference (FD) equations to obtain the numerical solution to the fundamental carrier currents $I(x, \omega_1)$ and $I(x, \omega_2)$. For a lossless and 50- Ω microstrip line with a length of 300 mm, both the analytical and numerical solutions of fundamental carrier current in the frequency domain at frequency f = 900 MHz are shown in Fig. 4.

The numerical solution to the nonlinear harmonic current $I(x, 2\omega_1 - \omega_2)$ and voltage $U(x, 2\omega_1 - \omega_2)$ can be obtained by combining (1) and (4) with the solutions to the fundamental carrier currents, which are then used to derive the PIM products. This model can be verified by the conclusion that as the length of the microstrip transmission line increases, the forward nonlinear waves are constructively interfered with when propagating, leading to a monotonic increase of PIM products. Conversely, the scattered reverse nonlinear wave propagates with destructive interference, causing the oscillation of PIM products [25].

C. Self-Consistency Solution to the Nonlinear Model

The contribution of nonlinear harmonic components to the generation of fundamental carrier components is neglected in the solution process of fundamental carrier currents $I(x, \omega_1)$ and $I(x, \omega_2)$. In fact, a more rigorous solution to the nonlinear harmonic current $I(x, 2\omega_1 - \omega_2)$ can be obtained if those contributions are considered. It is known that the contribution of harmonics to the fundamental components becomes weaker

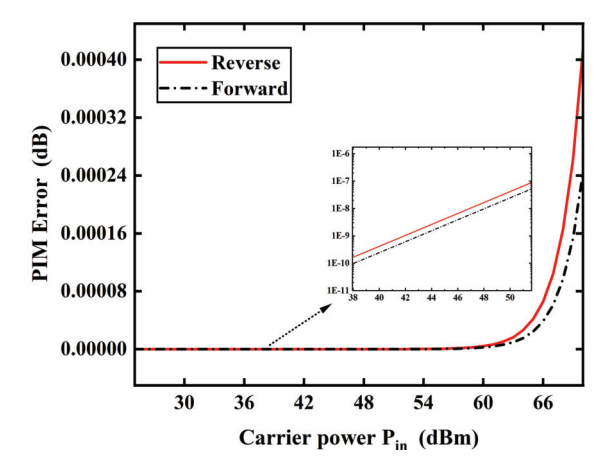


Fig. 5. Errors in reverse and forward PIMs between self-consistent and nonself-consistent solutions in the microstrip transmission line and the correction errors of PIM increase with the rising carrier power.

as the order of harmonics increases. Therefore, just the contributions of $I(x, 2\omega_1 - \omega_2)$ and $I(x, 2\omega_2 - \omega_1)$ to the generation of fundamental carrier currents need to be considered. The corrected fundamental current $I(x, \omega_1)$ satisfies the following equations:

$$\left. \frac{\partial U(x,\omega)}{\partial x} \right|_{\omega_1} = -(R_0 + j\omega L_0)I(x,\omega) - U_{\text{ns1}}$$
 (14)

$$\frac{\partial U(x,\omega)}{\partial x}\bigg|_{\omega_{1}} = -(R_{0} + j\omega L_{0})I(x,\omega) - U_{\text{ns1}} \qquad (14)$$

$$\frac{\partial I(x,\omega)}{\partial x}\bigg|_{\omega_{1}} = -(G_{0} + j\omega C_{0})U(x,\omega) \qquad (15)$$

where the distributed voltage source generated by mixing of harmonic and fundamental current components is given by

$$U_{\rm ns1} = R_n I^* (x, 2\omega_2 - \omega_1) I(x, \omega_2) I(x, \omega_2). \tag{16}$$

The corrected fundamental current $I(x, \omega_2)$ satisfies the following equations:

$$\frac{\partial U(x,\omega)}{\partial x}\bigg|_{\text{cr}} = -(R_0 + j\omega L_0)I(x,\omega) - U_{\text{ns}2}$$
 (17)

$$\frac{\partial U(x,\omega)}{\partial x}\bigg|_{\omega_2} = -(R_0 + j\omega L_0) I(x,\omega) - U_{\text{ns2}} \qquad (17)$$

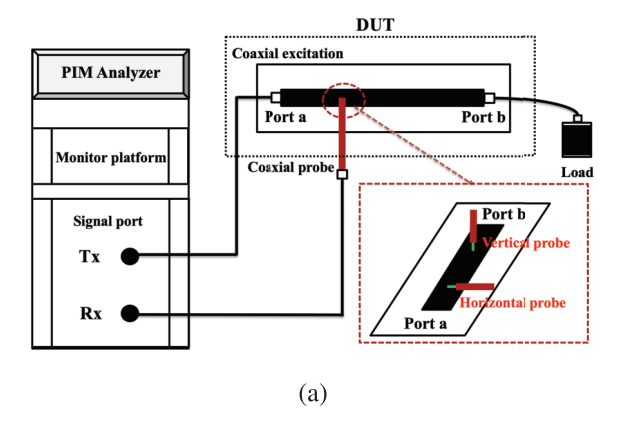
$$\frac{\partial I(x,\omega)}{\partial x}\bigg|_{\omega_2} = -(G_0 + j\omega C_0) U(x,\omega) \qquad (18)$$

where the distributed voltage source is

$$U_{\rm ns2} = R_n I^* (x, 2\omega_1 - \omega_2) I(x, \omega_1) I(x, \omega_1). \tag{19}$$

The boundary conditions for the calculation of fundamental carrier components are the same as in (12) and (13). The corrected fundamental carrier currents are coupled into the nonlinear equation to update the solution to the nonlinear harmonic current $I(x, 2\omega_1 - \omega_2)$, thereby providing a more rigorous self-consistent solution for PIM products.

The simulation is performed for a lossless and perfectly matched microstrip transmission line with a length of 300 mm, where the carrier frequencies are $f_1 = 930$ MHz and $f_2 = 950$ MHz. The errors in reverse and forward PIMs between self-consistent and nonself-consistent solutions are shown in Fig. 5. It can be observed that the correction errors of PIM increase with the rising carrier power. From the selfconsistent solution, the nonlinear coupled transmission line



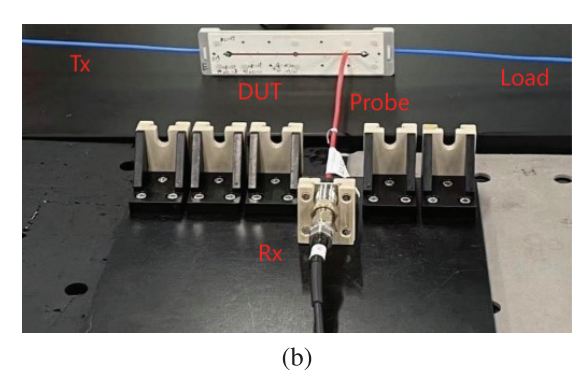


Fig. 6. Experimental setup of the near-field measurements for PIM distribution in microstrip transmission lines. (a) Schematic of near-field measurements for PIM distribution. The microstrip transmission line under test is terminated with a low PIM-matched load and Tx port of the PIM analyzer, and the coaxial probe is connected to the RX port of the PIM analyzer. (b) Testing environment of near-field measurements for PIM distribution in microstrip transmission lines.

model could satisfy the energy-conservation law compared to the nonself-consistent version.

III. EXPERIMENTAL VALIDATION OF NONLINEAR MODEL

To validate the developed nonlinear coupled-wave model, simulation results from the nonlinear coupled-wave model are compared to the near-field measurements data along the microstrip transmission line [25]. The near-field measurement technique follows the methods outlined in [34] and [35], and the experimental equipment for calibration and near-field measurement includes a PIM analyzer, a vector network analyzer (VNA), an ideal load, and a coaxial capacitive probe, as shown in Fig. 6. The experimental test process is given as follows. First, the probe is connected to the input of the PIM analyzer to measure the residual PIM of the probe. The VNA is then used to measure the S parameters to determine the disturbance and coupling of the probe. Finally, the microstrip transmission line under test is terminated with the Tx port of the PIM analyzer and the matched load, respectively. The coaxial probe is connected to the Rx port of the PIM analyzer to measure the PIM distribution of the microstrip transmission line. Both vertical and horizontal probes are used to ensure consistency in the PIM trend across different directions and minimize probeinduced interference with the PIM measurements.

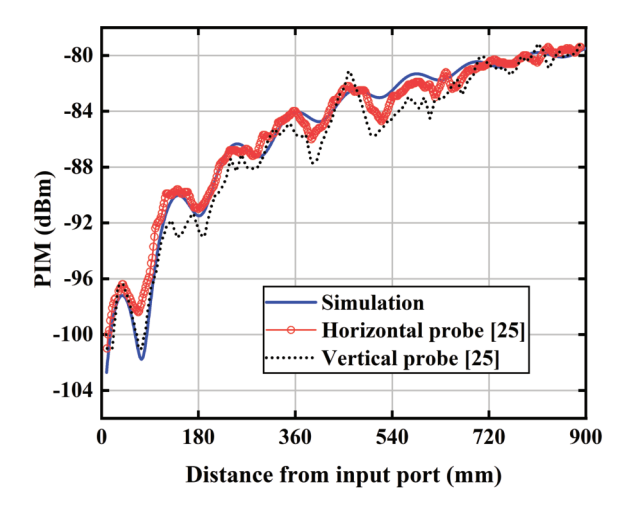


Fig. 7. Comparison of PIM distribution from simulation and near-field measurement [25] along the microstrip transmission line. The near-field PIM results are measured by the vertical probe and the horizontal probe, respectively.

TABLE I
PARAMETERS OF THE MICROSTRIP TRANSMISSION LINE UNDER
NEAR-FIELD MEASUREMENT [25]

length (mm)	thickness (mm)	impedance (Ω)	ϵ_r	$tan\delta$
914	0.76	50	3	0.0026

The parameters of the microstrip transmission line to be measured are listed in Table I, including the length and impedance of the microstrip transmission line, the thickness of substrate board, the dielectric constant ϵ_r , and the loss tangent $\tan \delta$ of substrate board. The microstrip transmission line is fed by two 44-dBm carriers at frequencies $f_1 = 935$ MHz and $f_2 = 960$ MHz. After the test is completed, the measured PIM needs to be corrected by subtracting the coupling degree of the probe. The PIM distribution obtained by both the measurement and simulation is shown in Fig. 7, and the maximum error at each test point is less than ± 5 dB.

The simulation results are derived from the self-consistent modified model, which accounts for the contribution of nonlinear harmonic components to the generation of the fundamental carrier component. The value of the nonlinear resistance $R_n = 9.5 \times 10^{-2} \ \Omega \cdot \text{A}^{-3} \cdot \text{m}^{-1}$ has been calculated to equalize the power levels in the simulations and near-field measurements at each position. The PIM fluctuation measured by the vertical probe is larger than that of the horizontal probe because the vertical and horizontal probes have different interference and coupling degrees on the field distribution at different positions.

In addition, reverse and forward PIM measurements at f = 910 MHz are carried out on various microstrip transmission lines. The microstrip transmission lines are terminated with the Tx and Rx ports of the PIM analyzer to measure the reverse and forward PIMs, and the structural parameters are listed in Table II. To avoid the time-varying nature of PIM and minimize fluctuations caused by factors such as the test environment, five times measurements are conducted on each microstrip line and averaged the results to ensure stability, and the optimal R_n value is determined by simultaneously

TABLE II

PARAMETERS OF MICROSTRIP LINE UNDER TEST
FOR REVERSE AND FORWARD PIMS

length (mm)	thickness (mm)	impedance (Ω)	ϵ_r	$tan\delta$
154	1.5	50	4	0.004

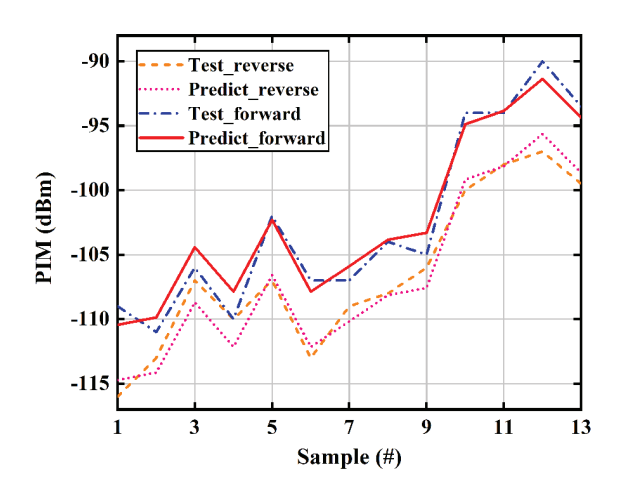


Fig. 8. Comparison of the simulation and measurement for the reverse and forward PIMs in various microstrip transmission lines. The prediction errors of forward and reverse PIMs are less than 3 dB.

minimizing errors between the average test results and the simulation results of both the reverse and forward PIMs. The comparison of simulation and measurement results for reverse and forward PIMs in various samples is shown in Fig. 8. The results show that the prediction errors for both reverse and forward PIMs on various microstrip lines fall within a range of ± 3 dB. The test samples exhibit significant variations in PIM levels due to differences in the manufacturing processes, such as varying roughness of metal lines.

IV. SIMULATION OF NONLINEAR COUPLED-WAVE MODELS IN 3-D MICROSTRIP LINES

The structural extension of the nonlinear coupled-wave model is mainly discussed in this section, including the verification of the nonlinear coupled-wave model with full-wave simulation in multiphysics software COMSOL, the comparison of PIM distribution between straight and bent microstrip transmission lines, and the impact of bending position on PIM distribution.

A. Model Verification With Full-Wave Simulation

The nonlinear coupled-wave model based on the uniform transmission line equation is limited to predict the PIM products in uniform microstrip transmission lines, and the extraction errors in parameters R_0 , L_0 , G_0 , and G_0 significantly affect the PIM calculation in the nonlinear coupled-wave model. Therefore, the structural extension of the nonlinear model is necessary. Similar to HFSS, commercial software COMSOL employs the finite element method (FEM) to solve Maxwell's equations based on boundary conditions and is more capable of incorporating distributed nonlinear sources.

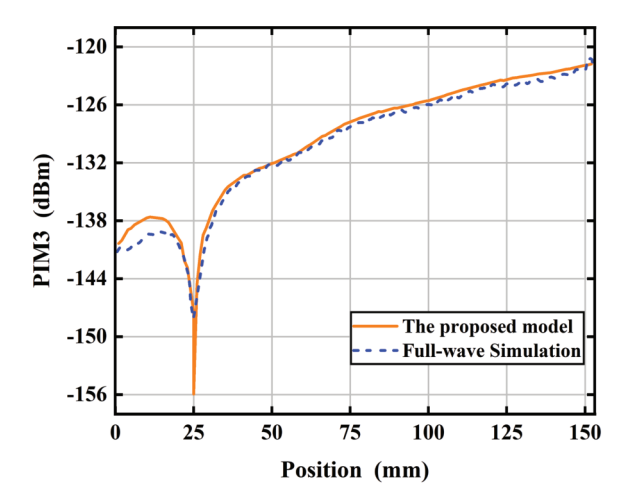


Fig. 9. Distribution of PIM products along the microstrip line calculated by nonlinear coupled-wave model and full-wave simulation in COMSOL. Lower PIM levels are observed at specific locations due to the interference between nonlinear sources and phase matching.

Therefore, the proposed solution in the frequency domain can be applied to COMSOL for low-PIM design and optimization in special structures and topologies of microstrip transmission lines.

The nonlinear modeling method in COMSOL comprises the following steps. First, the structure of the microstrip transmission line is built, and Maxwell's equations are subsequently employed to conduct a full-wave simulation for solving the electric field distribution of fundamental carrier components $E(x, \omega_1)$ and $E(x, \omega_2)$. Second, the obtained fundamental carrier electric fields are utilized to calculate the nonlinear harmonic current source by the following formula:

$$J(x, 2\omega_1 - \omega_2) = \sigma_n E(x, \omega_1) E(x, \omega_1) E^*(x, \omega_2)$$
 (20)

where σ_n is the nonlinear conductivity, which is a microscopic representation of R_n in the nonlinear coupled-wave model. Third, the distributed nonlinear sources are incorporated into the microstrip transmission line by setting the scattering boundary conditions and introducing external current density in COMSOL. Finally, a full-wave simulation in the frequency domain is performed to calculate the nonlinear harmonic voltage and current at intermodulated frequency. The PIM distribution along the straight microstrip transmission line with the parameters listed in Table II is obtained using COMSOL and the nonlinear coupled-wave model, as shown in Fig. 9. The deep notch at 25 mm is caused by the mutual interference of nonlinear waves with different phases generated by the nonlinear source. This phenomenon can be explained by the four-wave mixing theory [25].

The simulation results from COMSOL are consistent with those from the nonlinear coupled-wave model, indicating the possibility of the nonlinear model for structural extension. The slight differences originate from the differences in the dimensions of the microstrip lines and the extraction accuracy of the RLCG element parameters in the nonlinear coupled wave model. Lower PIM levels are observed at specific locations due to the interference between nonlinear sources and phase matching.

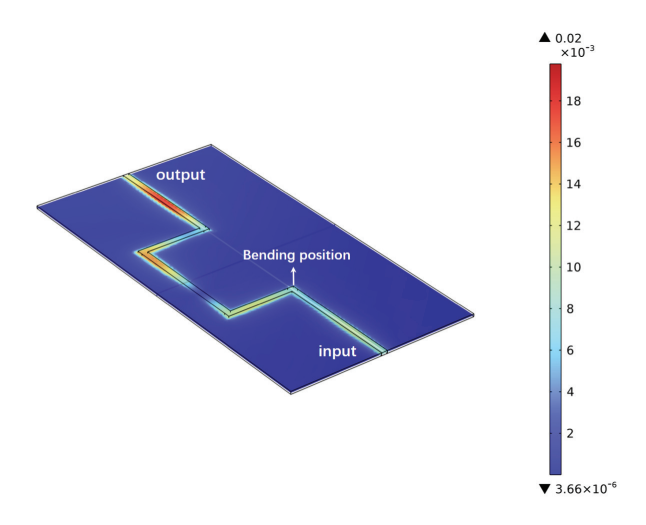


Fig. 10. Structure of the bent microstrip line and the corresponding electric field at the intermodulated frequency calculated in COMSOL.

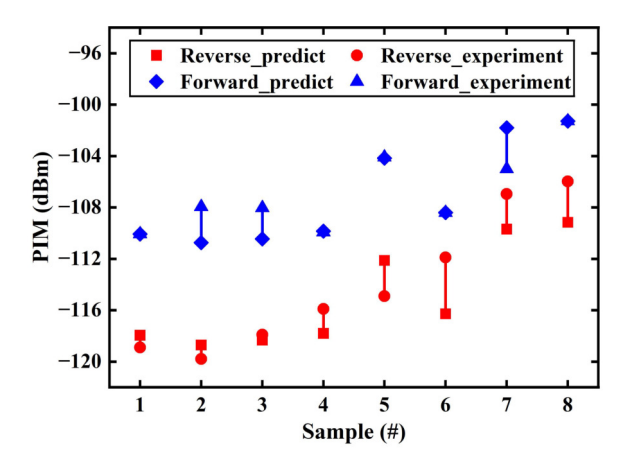


Fig. 11. Comparison of the simulation and measurement for the reverse and forward PIMs in various bent microstrip transmission lines. The prediction errors of forward and reverse PIMs are less than 5 dB.

B. Structural Extension of Nonlinear Model

In practical circuits, microstrip transmission lines commonly have bent structures to reduce circuit area or fit a specific design. Since the reverse and forward PIMs vary significantly with the reflection coefficient [25], the bent microstrip line will produce reflections at the corners, which may affect the distribution of PIM. The structure of the bent microstrip line and the electric field in COMSOL with the design parameters listed in Table II are shown in Fig. 10. The PIM distribution of curved microstrip lines is significantly different from the PIM distribution of straight microstrip lines [36]. Moreover, the reverse and forward PIMs of eight bent microstrip lines are measured at f = 900 MHz to demonstrate the accuracy of the proposed model, as shown in Fig. 11.

The different bending positions may also influence the spatial distribution of standing waves in the bent microstrip line, subsequently affecting the intensity of the nonlinear sources. For a bent microstrip transmission line with the parameter listed in Table II, the total length of the substrate is 457.8 mm, and the length between the two bending points is 57.8 mm. The impacts of the bending position on the

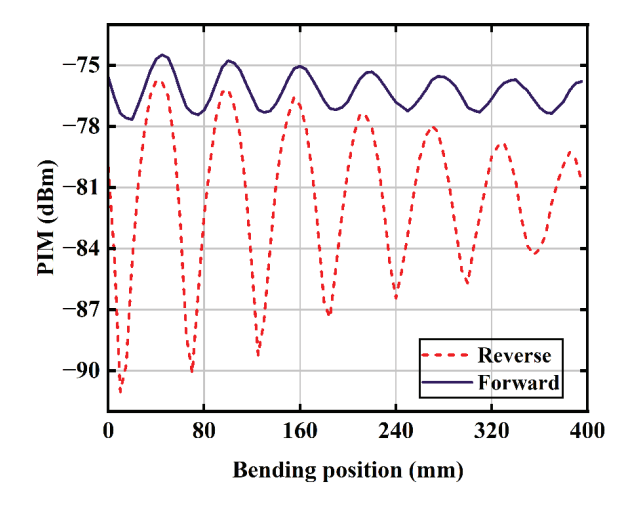


Fig. 12. Impacts of the bending position in the bent microstrip line on the reverse and forward PIMs at the ports. Both reverse and forward PIMs oscillate at half the wavelength, and the oscillation amplitude decreases as the distance between the bending position and the input port increases.

reverse and forward PIMs at the intermodulated frequency f = 2.596 GHz are shown in Fig. 12. For different bending positions, both the reverse and forward PIMs oscillate with a period of half the wavelength. The amplitude of forward PIM is slightly affected by the bending position because the forward nonlinear wave propagates with constructive interference, but it is also affected by the reflected waves and oscillates with the bending position. However, the amplitude of the reverse PIM is significantly affected by the bending position because the scattered reverse nonlinear waves propagate in a destructive interference manner, and the loss and reflection levels at different bending positions also affect the reverse PIM. Therefore, it is necessary to choose a suitable bending position so that both reverse and forward PIMs are at low levels in the bent microstrip lines.

V. CONCLUSION

In this article, a rigorously formulated distributed nonlinear source is proposed based on nonlinear mixing theory, which is then incorporated into the transmission line equations to establish the nonlinear coupled-wave model in the frequency domain. Furthermore, a self-consistent method is proposed to solve the nonlinear model, and the FDM is used to reduce computational complexity. The validity of the theoretical model is confirmed by the good agreements between predictions and results obtained from near-field measurements and tests of reverse and forward PIMs on a series of microstrip transmission lines. Subsequently, the consistency between the PIM distribution of the uniform microstrip line from fullwave simulation and the nonlinear coupled-wave model is verified, and the extended full-wave model works well for the modeling of bent microstrip transmission lines. Finally, the PIM distribution of the bent microstrip transmission line and the influence of bending position on the PIM distribution are discussed, thus providing guidance for the structural design and optimization of low-PIM microstrip transmission lines.

REFERENCES

- Z. Cai, L. Liu, F. de Paulis, and Y. Qi, "Passive intermodulation measurement: Challenges and solutions," *Engineering*, vol. 14, pp. 181–191, Jul. 2022.
- [2] D. Yang, T. Liu, and Y. Ye, "Ferrite isolator design with low intermodulation distortion under high power condition," in *Proc. 6th Int. Conf. Wireless Commun. Netw. Mobile Comput. (WiCOM)*, Chengdu, China, Sep. 2010, pp. 1–4.
- [3] J. E. Erickson, "Intermodulation reduction in VHF communications systems," Griffiss Air Force Base, New York, NY, Tech. Rep. AD-AO17 486, Sep. 1975.
- [4] T. Miura and L. E. Davis, "Evaluation of intermodulation distortion of a ferrite element by the two-tone method," *IEEE Trans. Microw. Theory Techn.*, vol. 57, no. 6, pp. 1500–1507, Jun. 2009.
- [5] T. Miura and L. Davis, "A study of ferrite nonlinearity evaluation from higher harmonic generation efficiency," in *Proc. Eur. Microw. Conf.*, Sep. 2006, pp. 917–920.
- [6] C. Vicente, D. Wolk, H. L. Hartnagel, B. Gimeno, V. E. Boria, and D. Raboso, "Experimental analysis of passive intermodulation at waveguide flange bolted connections," *IEEE Trans. Microw. Theory Techn.*, vol. 55, no. 5, pp. 1018–1028, May 2007.
- [7] X. Chen, L. Wang, D. Pommerenke, and M. Yu, "Passive intermodulation on coaxial connector under electro-thermal-mechanical multiphysics," *IEEE Trans. Microw. Theory Techn.*, vol. 70, no. 1, pp. 169–177, Jan. 2022.
- [8] J. Henrie, A. Christianson, and W. J. Chappell, "Prediction of passive intermodulation from coaxial connectors in microwave networks," *IEEE Trans. Microw. Theory Techn.*, vol. 56, no. 1, pp. 209–216, Jan. 2008.
- [9] H. Yang, L. Zhu, F. Gao, J. Fan, and H. Wen, "Measurement and analysis of passive intermodulation induced by additional impedance in loose contact coaxial connector," *IEEE Trans. Electromagn. Compat.*, vol. 61, no. 6, pp. 1876–1883, Dec. 2019.
- [10] Q. Jin, J. Gao, G. T. Flowers, Y. Wu, and G. Xie, "Modeling of passive intermodulation with electrical contacts in coaxial connectors," *IEEE Trans. Microw. Theory Techn.*, vol. 66, no. 9, pp. 4007–4016, Sep. 2018.
- [11] R. Wang, W. Cui, X. Chen, C. Bai, N. Zhang, and Y. Li, "Experimental analysis of passive intermodulation at TNC coaxial connectors," in *Proc.* 11th Eur. Conf. Antennas Propag. (EUCAP), Mar. 2017, pp. 2383–2386.
- [12] G. Macchiarella, G. B. Stracca, and L. Miglioii, "Experimental study of passive intermodulation in coaxial cavities for cellular base stations duplexers," in *Proc. 34th Eur. Microw. Conf.*, vol. 2, Oct. 2004, pp. 981–984.
- [13] B. Choi, "Experimental study on the practical mitigation of passive intermodulation for time and temperature in cavity duplexer," *Electron. Lett.*, vol. 57, no. 11, pp. 442–444, May 2021.
- [14] A. Moriya, M. Inoue, and O. Kawachi, "Development of high linearity duplexers with low passive intermodulation component," in *Proc. IEEE Int. Ultrason. Symp. (IUS)*, Prague, Czech Republic, Jul. 2013, pp. 737–740.
- [15] A. K. Brown, "Passive intermodulation products in antennas—An overview," in *Proc. IEE Passive Intermod. Products Antennas Relat.* Struct. Colloq., London, U.K., Jun. 1989, p. 1.
- [16] V. Golikov, S. Hienonen, and P. Vainikainen, "Passive intermodulation distortion measurements in mobile communication antennas," in *Proc. IEEE 54th Veh. Technol. Conf.*, Oct. 2001, pp. 2623–2625.
- [17] J. R. Wilkerson, I. M. Kilgore, K. G. Gard, and M. B. Steer, "Passive intermodulation distortion in antennas," *IEEE Trans. Antennas Propag.*, vol. 63, no. 2, pp. 474–482, Feb. 2015.
- [18] L. Chen, S. Lin, J. Qiu, X. Wang, and S. Fan, "Analysis and measurement of antenna passive intermodulation," in *Proc. Int. Conf. Electron. Inf. Eng.*, vol. 2, Kyoto, Japan, Aug. 2010, pp. V2-133–V2-135.
- [19] W. Wang, Y. Wang, W. Zang, H. Duan, W. Chen, and W. E. I. Sha, "Physical mechanisms of passive intermodulation: A short review," in *Proc. Int. Appl. Comput. Electromagn. Soc. Symp. (ACES-China)*, Dec. 2022, pp. 1–3.
- [20] D. S. Kozlov, A. P. Shitvov, A. G. Schuchinsky, and M. B. Steer, "Passive intermodulation of analog and digital signals on transmission lines with distributed nonlinearities: Modelling and characterization," *IEEE Trans. Microw. Theory Techn.*, vol. 64, no. 5, pp. 1383–1395, May 2016.
- [21] B. Nouri and M. Nakhla, "Efficient simulation of nonlinear transmission lines using empirical interpolation and projection-based model order reduction," in *IEEE MTT-S Int. Microw. Symp. Dig.*, Philadelphia, PA, USA, Jun. 2018, pp. 87–89.

- [22] L. Zhang, H. Wang, S. He, H. Wei, Y. Li, and C. Liu, "A segmented polynomial model to evaluate passive intermodulation products from low-order PIM measurements," *IEEE Microw. Wireless Compon. Lett.*, vol. 29, no. 1, pp. 14–16, Jan. 2019.
- [23] S. Hienonen and A. V. Räisänen, "Effect of load impedance on passive intermodulation measurements," *Electron. Lett.*, vol. 40, no. 4, pp. 245–247, Feb. 2004.
- [24] A. G. Schuchinsky, J. Francey, and V. F. Fusco, "Distributed sources of passive intermodulation on printed lines," in *Proc. Antennas Propag. Soc. Int. Symp.*, vol. 4B, Washington, DC, USA, Aug. 2005, pp. 447–450.
- [25] D. E. Zelenchuk, A. P. Shitvov, A. G. Schuchinsky, and V. F. Fusco, "Passive intermodulation in finite lengths of printed microstrip lines," *IEEE Trans. Microw. Theory Techn.*, vol. 56, no. 11, pp. 2426–2434, Nov. 2008.
- [26] D. Zelenchuk, A. P. Shitvov, A. G. Schuchinsky, and T. Olsson, "Passive intermodulation on microstrip lines," in *Proc. Eur. Microw. Conf.*, Munich, Germany, Oct. 2007, pp. 396–399.
- [27] J. R. Wilkerson, P. G. Lam, K. G. Gard, and M. B. Steer, "Distributed passive intermodulation distortion on transmission lines," *IEEE Trans. Microw. Theory Techn.*, vol. 59, no. 5, pp. 1190–1205, May 2011.
- [28] E. Rocas et al., "Passive intermodulation due to self-heating in printed transmission lines," *IEEE Trans. Microw. Theory Techn.*, vol. 59, no. 2, pp. 311–322, Feb. 2011.
- [29] P. Ansuinelli, A. G. Schuchinsky, F. Frezza, and M. B. Steer, "Passive intermodulation due to conductor surface roughness," *IEEE Trans. Microw. Theory Techn.*, vol. 66, no. 2, pp. 688–699, Feb. 2018.
- [30] Z. Cao et al., "Passive intermodulation on microstrip induced by microstructured edge," *IEEE Trans. Microw. Theory Techn.*, vol. 72, no. 3, pp. 1489–1502, Mar. 2024.
- [31] R. W. Boyd, Nonlinear Optics, 3rd ed., New York, NY, USA: Academic, 2020.
- [32] A. Shitvov, D. Zelenchuk, and A. Schuchinsky, "Experimental observations of distributed nonlinearity in printed transmission lines," in *Proc.* 14th Int. Microw. Opt. Appl. Novel Phys. Phenomena., Belfast, U.K., Nov. 2007, pp. 70–72.
- [33] K. S. Kunz and R. J. Luebbers. The Finite Difference Time Domain Method for Electromagnetics. Boca Raton, FL, USA: CRC Press, 1993.
- [34] A. P. Shitvov, D. D. Zelenchuk, A. G. Schuchinsky, V. F. Fusco, and N. Buchanan, "Mapping of passive intermodulation products on microstrip lines," in *IEEE MTT-S Int. Microw. Symp. Dig.*, Jun. 2008, pp. 1573–1576.
- [35] S. Hienonen and A. V. Räisänen, "Passive intermodulation near-field measurements on microstrip lines," in *Proc. 34th Eur. Microw. Conf.*, vol. 2, Amsterdam, The, Netherlands, Jan. 2004, pp. 1041–1044.
- [36] A. P. Shitvov, T. Olsson, B. E. Banna, D. E. Zelenchuk, and A. G. Schuchinsky, "Effects of geometrical discontinuities on distributed passive intermodulation in printed lines," *IEEE Trans. Microw. Theory Techn.*, vol. 58, no. 2, pp. 356–362, Feb. 2010.



Wenbo Wang received the B.S. degree from Nanjing University of Information Science and Technology, Nanjing, China, in 2019. He is currently pursuing the Ph.D. degree in electronic science and technology at Zhejiang University, Hangzhou, China.

His current research interests include passive intermodulation, RF integrated circuit designs, signal integrity in RRAM-based neuromorphic chips, and multiphysics modeling.



Wenchao Chen (Senior Member, IEEE) received the B.E. degree in information engineering from Xi'an Jiaotong University, Xi'an, China, in 2006, the M.E. degree in electronic engineering from Shanghai Jiao Tong University, Shanghai, China, in 2009, and the Ph.D. degree in electrical and computer engineering from the University of Florida, Gainesville, FL, USA, in 2014.

He is an Associate Professor with ZJU-UIUC Institute, Zhejiang University, Haining, China. His research interests include computational electromag-

netics, signal integrity analysis, multiphysics modeling and simulation of emerging electronic devices, and 3-D ICs.

Dr. Chen received the Natural Science Foundation of China (NSFC) for Excellent Young Scholars in 2021 and Zhejiang Provincial Natural Science Foundation for Outstanding Young Scholars in 2020.



Yimin Wang received the B.S. and M.S. degrees from Zhejiang University, Hangzhou, China, in 2019 and 2023, respectively.

His current research interests include passive intermodulation, nanotransistor reliability, and artificial intelligence for microwave technology.



Huali Duan received the B.S. degree from the Huazhong University of Science and Technology, Wuhan, China, in 2018, and the Ph.D. degree in electronic science and technology from Zhejiang University, Hangzhou, China, in 2024.

Her current research interests include computational electromagnetics, quantum transport, and multiphysics simulation of nanotransistors.



Shuai S. A. Yuan (Graduate Student Member, IEEE) received the B.E. degree from Nanjing University of Aeronautics and Astronautics, Nanjing, China, in 2019, and the Ph.D. degree in electronic science and technology from Zhejiang University, Hangzhou, China, in 2024.

From 2023 to 2024, he was a Visiting Ph.D. Student at the ELEDIA Research Center, University of Trento, Trento, Italy. His current research interests include electromagnetic methods for wireless communications, antenna arrays, and metasurfaces.



Wei E. I. Sha (Senior Member, IEEE) received the B.S. and Ph.D. degrees in electronic engineering from Anhui University, Hefei, China, in 2003 and 2008, respectively.

From July 2008 to July 2017, he was a Post-Doctoral Research Fellow and later a Research Assistant Professor at the Department of Electrical and Electronic Engineering, University of Hong Kong, Hong Kong. From March 2018 to March 2019, he held a Marie Skłodowska-Curie Individual Fellowship at the University College London, Lon-

don, U.K. In October 2017, he joined the College of Information Science and Electronic Engineering, Zhejiang University, Hangzhou, China, where he is currently a tenured Associate Professor. He has authored or co-authored over 220 peer-reviewed journal articles, 180 conference papers, 12 book chapters, and two books. His work has been cited over 11 943 times on Google Scholar, with an H-index of 58. His research focuses on theoretical and computational electromagnetics, including computational and applied electromagnetics, nonlinear and quantum electromagnetics, micro- and nanooptics, and multiphysics modeling.

Dr. Sha is a Life Member of OSA. He received multiple awards, including the ACES-China Electromagnetics Education Ambassador Award in 2024, the ACES Technical Achievement Award in 2022, and the PIERS Young Scientist Award in 2021. He was selected for China's Thousand Talents Program for Distinguished Young Scholars in 2017 and received the Second Prize for Science and Technology from Anhui Provincial Government in 2015. Nine of his students have won best student paper awards. He has reviewed more than 60 technical journals and served on the technical program committees of over ten IEEE conferences. He is an Associate Editor of IEEE JOURNAL ON MULTISCALE AND MULTIPHYSICS COMPUTATIONAL TECHNIQUES, IEEE OPEN JOURNAL OF ANTENNAS AND PROPAGATION, IEEE ACCESS, and Electromagnetic Science.